

# Toward Efficient Spiking Transformers: Synapse Pruning Meets Synergistic Learning-Based Compensation

Hongze Sun<sup>1</sup>, Wuque Cai<sup>1</sup>, Duo Chen<sup>1</sup>, Shifeng Mao<sup>1</sup>, Jiayi He<sup>1</sup>, Zhenxing Wang<sup>1</sup>, Dezhong Yao<sup>1,\*</sup>,  
Daqing Guo<sup>1,\*</sup>

<sup>1</sup>Clinical Hospital of Chengdu Brain Science Institute, MOE Key Lab for NeuroInformation, China-Cuba Belt and Road Joint Laboratory on Neurotechnology and Brain-Apparatus Communication, School of Life Science and Technology, University of Electronic Science and Technology of China, Chengdu 611731, China.

\*Corresponding authors: dyao@uestc.edu.cn, dqguo@uestc.edu.cn

## Abstract

As a foundational architecture of artificial intelligence models, Transformer has been recently adapted to spiking neural networks with promising performance across various tasks. However, existing spiking Transformer (ST)-based models require a substantial number of parameters and incur high computational costs, thus limiting their deployment in resource-constrained environments. To address these challenges, we propose combining synapse pruning with a synergistic learning-based compensation strategy to derive lightweight ST-based models. Specifically, two types of tailored pruning strategies are introduced to reduce redundancy in the weight matrices of ST blocks: an unstructured  $L_1$ P method to induce sparse representations, and a structured DSP method to induce low-rank representations. In addition, we propose an enhanced spiking neuron model, termed the synergistic leaky integrate-and-fire (sLIF) neuron, to effectively compensate for model pruning through synergistic learning between synaptic and intrinsic plasticity mechanisms. Extensive experiments on benchmark datasets demonstrate that the proposed methods significantly reduce model size and computational overhead while maintaining competitive performance. These results validate the effectiveness of the proposed pruning and compensation strategies in constructing efficient and high-performing ST-based models.

## Introduction

The Transformer architecture (Vaswani et al. 2017) has emerged as a foundational backbone for a wide array of large language models (Achiam et al. 2023; Devlin et al. 2019; Touvron et al. 2023), owing to its strengths in modeling long-range dependencies, adaptability across multiple modalities, and high parallelism. Recently, researchers have extended Transformer architectures to spiking neural networks (SNNs), giving rise to spiking Transformer (ST)-based models (Zhou et al. 2023b; Yao et al. 2023a). By making targeted adaptations to the dynamics of spiking neurons, these models have demonstrated significant improvements across a variety of complex tasks (Yao et al. 2024; Zhou et al. 2024a). However, the ST is inherently a parameter-intensive architecture, where performance often correlates with the model size (Dosovitskiy et al. 2021), resulting in substantial computational and efficiency costs. Achieving parameter-efficient adaptations and low computational cost thus remains a critical challenges in this field.

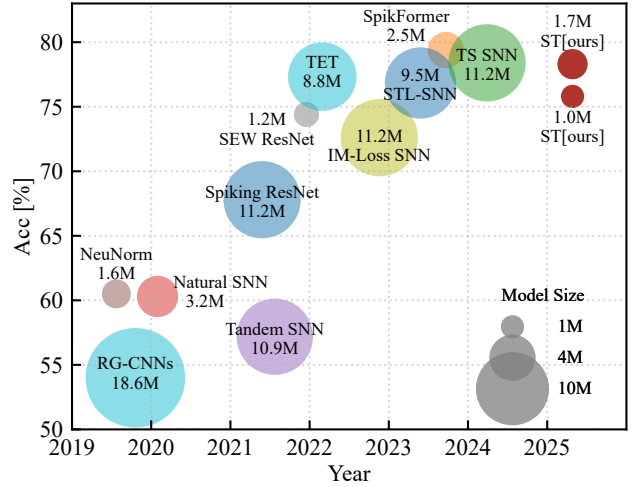


Figure 1: Comparison of model parameters and classification accuracy between our lightweight models and existing ST-based models on the CIFAR10-DVS dataset.

To enhance the efficiency of spatio-temporal (ST) blocks, numerous methods have been proposed in prior work. Among these, structure-oriented optimization represents a key direction, focusing on architectural modifications such as spatio-temporal pruning (Zhou et al. 2024b), meta-architecture redesign (Yao et al. 2024), and the integration of lightweight functional modules (Zhou et al. 2024a). These techniques aim to improve representational efficiency within ST blocks. Additionally, engineering-oriented approaches—such as quantization-aware training (Qiu et al. 2025) and specialized neuromorphic processors (Kim et al. 2025)—address practical concerns like energy consumption and inference latency, facilitating the deployment of ST-based models on resource-constrained edge devices. Despite their effectiveness, these approaches are often tightly coupled with specific model architectures or constrained by task-specific assumptions, limiting their generalizability (refer to Related Work in the Appendix for additional details). In contrast, our goal is to develop a universal, model-agnostic compression strategy for ST blocks without compromising performance.

SNNs are composed of biologically inspired spiking neu-

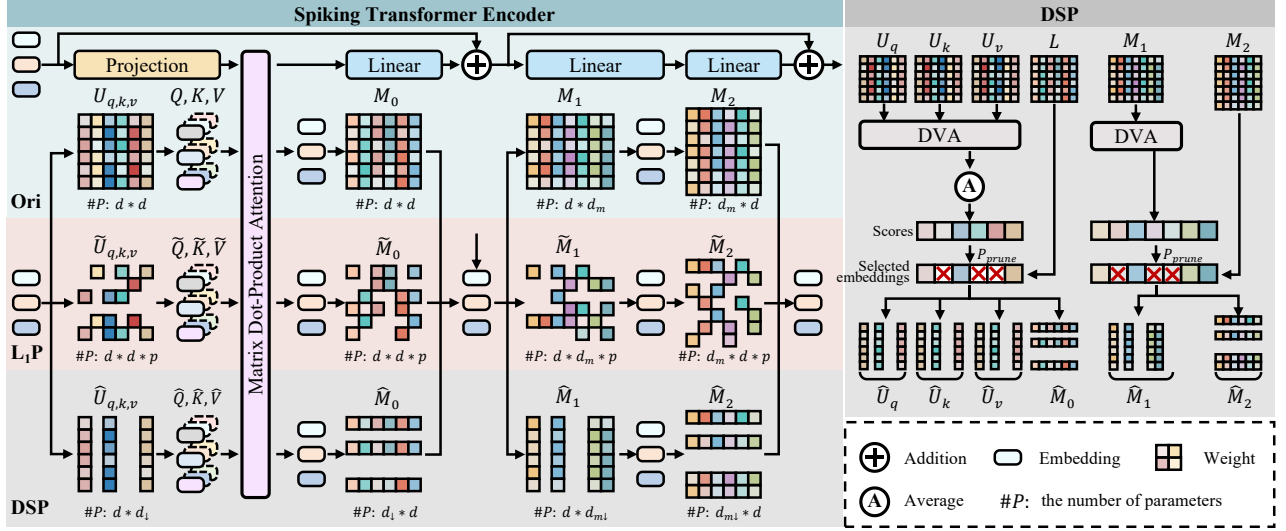


Figure 2: Overview of the proposed lightweight ST-based models and the associated pruning strategies.

rons that emulate the spatio-temporal dynamics observed in human brain activity. Drawing inspiration from these biological mechanisms, researchers have proposed a range of enhanced spiking neuron models (Qiu et al. 2025; Huang et al. 2024; Wang et al. 2023; Fang et al. 2021). Notably, models such as IE-LIF (Qiu et al. 2025), multi-threshold (Huang et al. 2024), and dynamic-threshold neurons (Wang et al. 2023) have been integrated into ST blocks to improve the efficiency of spiking units (see the Related Work in the Appendix for details). In this work, we aim to proposing an enhanced spiking neuron model that is efficient and simple to implement and train. We hope that the enhanced spiking neuron model can improve the efficiency of ST blocks, leading to more lightweight ST-based models.

To tackle the aforementioned challenges, we introduce a novel lightweight method that combines synapse pruning with a synergistic learning-based compensation strategy, aiming to construct lightweight yet high-performing ST-based models. We propose two types of customized pruning strategies tailored to the weight matrices within ST blocks: (1) an unstructured  $L_1$  norm-based parameter sparsification ( $L_1P$ ) method that promotes sparsity by removing weak synaptic connections, and (2) a structured dimension significance-based pruning (DSP) method that induces low-rank representations by reducing the dimensionality of patch embeddings. To mitigate the potential performance degradation caused by synapse pruning, we further introduce an enhanced spiking neuron model, termed the synergistic leaky integrate-and-fire (sLIF) neuron, which jointly leverages synaptic and intrinsic plasticity. Through synergistic learning between these two plasticity mechanisms, the sLIF neuron effectively compensates for the performance loss introduced by synapse pruning.

Our method address two key advantages. First, the pruning pipeline allows flexible control over model size by adjusting the desired sparsity level. Second, the proposed sLIF neuron is plug-and-play, enabling seamless integration into

existing ST-based models. As shown in Fig. 1, our approach achieves higher accuracy with fewer parameters compared to existing ST-based models on the neuromorphic CIFAR10-DVS dataset.

The contributions of this work are as follows:

- Two tailored pruning strategies are developed specifically for the ST block to enable efficient compression of ST-based models.
- An enhanced sLIF neuron model is proposed to effectively compensate for the information loss based on the synergistic learning between synaptic and intrinsic plasticity.
- Experiments across diverse tasks demonstrate that our method achieves significant model compression while maintaining competitive performance.

## Methods

In this section, we first propose two synapse pruning strategies tailored for spiking Transformers, encompassing both unstructured and structured approaches. Subsequently, we introduce an sLIF neuron model that concurrently incorporates synaptic and intrinsic plasticity, along with a compensation method based on synergistic learning.

### Efficient Compression for Spiking Transformer

A standard Spiking Transformer (ST) encoder can be formally described as follows:

$$x'_l = \text{SSA}(x_{l-1}) + x_{l-1}, \quad l = 1, \dots, L, \quad (1)$$

$$x_l = \text{MLP}(x'_l) + x'_l, \quad l = 1, \dots, L. \quad (2)$$

Here, the SSA and MLP represent the spiking self-attention module and linear layers module, respectively. In a ST-based model, the spatio-temporal patch embeddings  $x_0 \in \mathbb{R}^{T \times N \times d}$  are progressively refined through  $L$  stacked ST

blocks. The resulting high-level representations are subsequently fed into a task-specific prediction head to produce the final output.

Specifically, in the SSA module, the input  $x \in \mathbb{R}^{T \times N \times d}$ , consisting of  $N$  patch embeddings each of dimension  $d$ , is first linearly projected into query ( $Q$ ), key ( $K$ ), and value ( $V$ ) representations using three learnable projection matrices  $U_q \in \mathbb{R}^{d \times d}$ ,  $U_k \in \mathbb{R}^{d \times d}$  and  $U_v \in \mathbb{R}^{d \times d}$ , respectively:

$$[Q, K, V] = [xU_q, xU_k, xU_v]. \quad (3)$$

The attention output is computed using a scaled dot-product attention mechanism followed by a linear transformation:

$$x_{\text{attn}} = \frac{QK^T}{\sqrt{d}}V, \quad (4)$$

$$\text{SSA}(x) = x_{\text{attn}}M_0, \quad (5)$$

where  $M_0 \in \mathbb{R}^{d \times d}$  denotes the weight matrix of the post-attention linear layer. Subsequently, in the MLP module, two linear layers with weight matrices  $M_1 \in \mathbb{R}^{d \times d_m}$  and  $M_2 \in \mathbb{R}^{d_m \times d}$  are employed to generate the final output of the ST block:

$$\text{MLP}(x') = x'M_1M_2, \quad (6)$$

where  $d_m$  represents the hidden dimensionality of the MLP.

Two key observations are found in the ST block: (1) the majority of the parameter overhead arises from the matrices  $U_q$ ,  $U_k$ ,  $U_v$  and  $M_0$  in the SSA module, as well as  $M_1$  and  $M_2$  in the MLP module; and (2) as a task-independent, unified backbone for spatio-temporal feature extraction, the ST block presents a promising opportunity to develop universal lightweight strategies applicable across diverse downstream tasks. To this end, we propose two complementary pruning strategies—one unstructured and one structured—aimed at reducing the computational and memory complexity of the standard ST block.

**L<sub>1</sub> Norm-based Parameter Sparsification** Unstructured pruning offers a straightforward and flexible approach to model compression, with high implementation adaptability and demonstrated effectiveness in previous research. In our method, referred to as **L<sub>1</sub>P**, we prune by zeroing out a specified proportion of elements with the lowest L<sub>1</sub>-norm values within each target weight matrix. This strategy effectively reduces the number of model parameters while preserving the overall functional integrity of the network.

To mitigate potential degradation in model performance, the proposed **L<sub>1</sub>P** method performs pruning independently on each weight matrix. Let  $\mathbf{W} \in \mathbb{R}^{m \times n}$  denote a weight matrix, represented as  $\mathbf{W} = [w_{ij}]$  for  $i = 1, 2, \dots, m$  and  $j = 1, 2, \dots, n$ . The corresponding sparse matrix  $\widetilde{\mathbf{W}}$  is constructed through the following steps:

1. **Magnitude Computation:** Compute the element-wise absolute value matrix  $\mathbf{A}$ , where each element is given by:

$$A_{ij} = \|w_{ij}\|_1, \quad (7)$$

for  $i = 1, 2, \dots, m$  and  $j = 1, 2, \dots, n$ .

2. **Threshold Selection:** Determine the pruning threshold  $P_{\text{th}}$  based on a predefined pruning sparsity  $p \in [0, 1]$

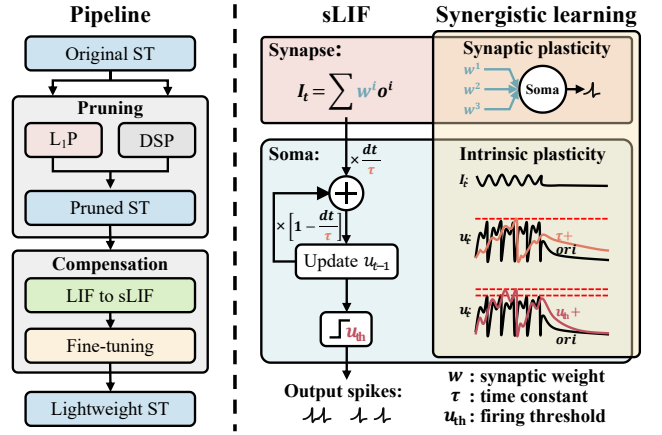


Figure 3: Illustration of the overall pipeline of the proposed method, including the sLIF neuron model and the synergistic learning mechanism.

as follows: (a) Sort all elements in  $\mathbf{A}$  in ascending order to obtain the sorted sequence  $\mathbb{V} = \{v_k \mid k = 1, 2, \dots, mn\}$ ; (b) Compute the index  $K = \lceil p \cdot mn \rceil$ , where  $\lceil \cdot \rceil$  denotes the ceiling function, and set the threshold as  $P_{\text{th}} = v_K$ .

3. **Pruning Operation:** Apply thresholding to obtain the sparse matrix  $\widetilde{\mathbf{W}}$ , where each element is updated as:

$$\widetilde{w}_{ij} = \begin{cases} w_{ij}, & \text{if } \|w_{ij}\|_1 \geq P_{\text{th}}, \\ 0, & \text{otherwise.} \end{cases} \quad (8)$$

This unstructured pruning approach retains weights with relatively larger magnitudes, thereby inducing sparsity while maintaining the model’s representational capacity.

**Dimension Significance-based Pruning** Structured pruning represents a more principled and architecture-aware strategy for model compression, wherein entire groups of weights are removed in a structured manner. This approach enables tangible improvements in inference efficiency and model compactness. Within a ST block, the weight matrices function as dimensional projectors, transforming input patch embeddings into a new representational space. Nevertheless, it remains unclear whether the extended dimensionality of patch embeddings is essential, and which specific dimensions can be pruned without significantly degrading performance.

Motivated by the preceding observations, we propose a Dimension Significance-based Pruning (**DSP**) method. The **DSP** approach employs a novel Dimension Value Assessment (DVA) metric to decompose the original weight matrix into low-rank representations by retaining dimension projectors associated with higher significance scores. Formally, for a weight matrix  $\mathbf{W} \in \mathbb{R}^{m \times n}$ , which maps an input dimension of size  $m$  to an output dimension of size  $n$ , the DVA metric computes the significance scores  $\mathbf{s} \in \mathbb{R}^n$  for each output dimension as follows:

$$s_j = \text{DVA}(\mathbf{W}) = \sum_{i=1}^m \|w_{ij}\|_1, \quad j = 1, \dots, n. \quad (9)$$

As illustrated in Fig. 2, for the SSA module, the significance scores  $\mathbf{s}_{\text{ssa}} \in \mathbb{R}^n$  are computed as the average DVA scores of the weight matrices  $\mathbf{U}_q, \mathbf{U}_k, \mathbf{U}_v \in \mathbb{R}^{d \times d}$ :

$$\mathbf{s}_{\text{ssa}} = \frac{1}{3} [\text{DVA}(\mathbf{U}_q) + \text{DVA}(\mathbf{U}_k) + \text{DVA}(\mathbf{U}_v)]. \quad (10)$$

Given a predefined pruning sparsity  $p \in [0, 1]$ , the  $[p \cdot n]$  dimensions with the lowest significance scores are pruned from the weight matrices  $\mathbf{U}_q, \mathbf{U}_k$ , and  $\mathbf{U}_v$ , yielding low-rank projectors  $\hat{\mathbf{U}}_q, \hat{\mathbf{U}}_k, \hat{\mathbf{U}}_v \in \mathbb{R}^{d \times d_\downarrow}$ , where  $d_\downarrow = n - [p \cdot n]$ . Subsequently, by pruning the corresponding input dimensions, a low-rank matrix  $\hat{\mathbf{M}}_0 \in \mathbb{R}^{d_\downarrow \times d}$  is obtained. Similarly, for the weight matrices  $\mathbf{M}_1, \mathbf{M}_2 \in \mathbb{R}^{d \times d}$  in the MLP module, an analogous pruning process is applied to obtain low-rank matrices  $\hat{\mathbf{M}}_1 \in \mathbb{R}^{d \times d_{m\downarrow}}$  and  $\hat{\mathbf{M}}_2 \in \mathbb{R}^{d_{m\downarrow} \times d}$ .

### Synergistic Learning-based Compensation

The overall pipeline of our proposed method is illustrated in Fig. 3, encompassing both synapse pruning and information compensation. Initially, a pre-trained original ST is pruned using either the  $L_1P$  or DSP strategy, yielding a pruned model. Subsequently, the original neurons are replaced with sLIF neurons, followed by fine-tuning via synergistic learning to mitigate information loss and produce a lightweight ST block.

Various spiking neuron models have been proposed to mimic the spatio-temporal dynamics of biological neurons. Among them, the LIF model is widely used in SNNs due to its balance between biological fidelity and computational efficiency. With surrogate gradient methods like spatio-temporal backpropagation (STBP), SNNs have shown notable performance in learning complex patterns. However, most studies focus on synaptic plasticity, neglecting the role of intrinsic neuronal parameters in modulating excitability. To bridge this gap, we propose the sLIF model, which integrates synaptic and intrinsic plasticity (IP) into a unified learning framework.

The dynamics of the proposed sLIF neuron are governed by the following differential equation:

$$\tau \frac{du_t}{dt} = -(u_t - u_{\text{rest}}) + I_t, \quad (11)$$

where  $u_t$  denotes the membrane potential at time  $t$ ,  $u_{\text{rest}}$  is the resting potential, and  $I_t$  is the total synaptic input current received by the neuron. The generation of output spikes follows a thresholding mechanism:

$$o_t = H(u_t - u_{\text{th}}), \quad (12)$$

where  $H(\cdot)$  denotes the Heaviside step function, and  $u_{\text{th}}$  is the firing threshold. The synaptic input  $I_t$  is computed as the weighted summation of incoming spikes:

$$I_t = \sum_i I_{\text{syn}}^{i,t} = \sum_i w^i o^{i,t}, \quad (13)$$

where  $w^i$  and  $o^{i,t}$  represent the synaptic weight and the presynaptic spike from the  $i$ -th neuron at time  $t$ , respectively.

Distinct from prior models, the sLIF neuron treats intrinsic parameters, the membrane time constant  $\tau$  and the firing

threshold  $u_{\text{th}}$ , as learnable parameters, and optimizes them alongside the synaptic weights  $w$ . As illustrated in Fig. 3, the membrane time constant determines the rate at which historical information is forgotten, while the firing threshold directly influences the neuron’s firing rate. The synergistic learning between synaptic and intrinsic parameters enhances neuronal heterogeneity, thereby improving the representational capacity of the SNN models.

To mitigate the performance degradation induced by synapse pruning, the LIF neurons in the ST blocks are replaced with the proposed sLIF neuron model. Subsequently, the pruned model is fine-tuned using synergistic learning over a small number of epochs. To facilitate efficient adaptation, the synaptic and intrinsic parameters are initialized by transferring them from the original model.

## Experiments and Results

### Experimental Settings

To evaluate the effectiveness of our method, experiments are conducted on both static and neuromorphic image datasets, ImageNet (Deng et al. 2009), CIFAR-10 (Krizhevsky, Hinton et al. 2009), and CIFAR10-DVS (Li et al. 2017). To further validate the generalization capability in downstream tasks, semantic segmentation is performed on the ADE20K dataset (Zhou et al. 2017). For a fair comparison, our method are directly applied to state-of-the-art (SOTA) pre-trained models implemented using the PyTorch and SpikingJelly frameworks (Zhou et al. 2023b; Yao et al. 2024; Fang et al. 2023). All experiments are executed on 4 NVIDIA A800 GPUs. The details can be seen in the Appendix.

### Comparisons with SOTA Methods

**Static Datasets Classification** We present our resulting lightweight models against other SNNs on the ImageNet-100 dataset (Tab. 1). The Spikformer-8-512-2048 model is selected as the baseline, which comprises 8 ST blocks with  $d = 512$  and  $d_m = 2048$ . Following pruning with a sparsity level of  $p = 90\%$ , the number of model parameters is significantly reduced to below 7M, achieving a compression ratio (CR) exceeding 77%, while incurring only a minor drop in classification accuracy ( $-3.14\%$  for  $L_1P$ +sLIF and  $-2.48\%$  for DSP+sLIF). When considering only the ST blocks, the CR exceeds 90%, with parameters reduced to below 2.5M. When the sparsity is substantially increased to an extreme value of  $p = 99\%$ , the classification accuracy exhibits an approximate degradation of 16%. However, given that the parameter count of the ST blocks is reduced from 24M to just 0.25M and 0.24M, the performance trade-off remains acceptable for lightweight deployment. Furthermore, compared to ResNet- or VGG-based convolutional models with comparable accuracy, our lightweight models still demonstrate significantly higher parameter efficiency.

On the CIFAR10 dataset (Tab. 2), ST-based models such as Spikformer and CML exhibit superior performance, with CML attaining the highest accuracy of 96.04% when employing the Spikformer-4-384-1536 architecture. Utilizing our proposed  $L_1P$ +sLIF method, an accuracy of 93.94% is achieved under a sparsity level of  $p = 80\%$ , accompanied

Method	Architecture	p [%]	CR [%]	Param [M]	Accuracy [%]
LOCALZO+TET (Mukhoty et al. 2023)	SEWResNet34	-	-	63.47	78.58
IM-SNN (Hasssan et al. 2024)	Resnet34	-	-	21.27	74.42
IMP+TET (Shen et al. 2024)	SEW-ResNet18	-	-	63.47	78.70
EfficientLIF-Net (Kim et al. 2023)	VGG16	-	-	23.52	73.22
Spikformer <sup>†</sup> (Zhou et al. 2023b)	Spikformer-8-512-2048	-	-	29.24/25.17	<b>79.36</b>
L <sub>1</sub> P+sLIF (ours)	Spikformer-8-512-2048	90	77.43/89.99	6.60/2.52	76.22(-3.14)
L <sub>1</sub> P+sLIF (ours)	Spikformer-8-512-2048	99	85.19/99.00	<b>4.33/0.25</b>	62.76(-16.60)
DSP+sLIF (ours)	Spikformer-8-48-204	90	77.63/90.46	6.54/2.40	76.88(-2.48)
DSP+sLIF (ours)	Spikformer-8-8-20	99	85.05/99.05	4.37/0.24	62.76(-16.60)

Table 1: Classification results on the ImageNet-100 dataset. The symbol <sup>†</sup> denotes the baseline model. The terms p and CR indicate the pruning sparsity and compression ratio, respectively. The notation ‘/’ separates values measured on the entire model and on the ST blocks.

Dataset	Method	Architecture	p [%]	CR [%]	Param [M]	Accuracy [%]
CIFAR10	STBP-tdBN (Zheng et al. 2021)	ResNet-19	-	-	11.17	92.92
	STP (Ma et al. 2025)	ResNet18	-	-	63.47	94.86
	STL-SNN (Sun et al. 2023)	ConvFC	-	-	11.37	92.42
	Spikformer <sup>†</sup> (Zhou et al. 2023b)	Spikformer-4-384-1536	-	-	9.32/7.08	95.19
	CML (Zhou et al. 2023a)	Spikformer-4-384-1536	-	-	9.32/7.08	<b>96.04</b>
	L <sub>1</sub> P+sLIF (ours)	Spikformer-4-384-1536	80	60.62/79.94	3.67/1.42	93.94(-1.25)
	L <sub>1</sub> P+sLIF (ours)	Spikformer-4-384-1536	90	68.24/89.97	<b>2.96/0.71</b>	92.32(-2.87)
	DSP+sLIF (ours)	Spikformer-4-84-307	80	60.19/79.38	3.71/1.46	93.14(-2.05)
	DSP+sLIF (ours)	Spikformer-4-48-153	90	67.60/89.12	3.02/0.77	92.23(-2.96)
CIFAR10-DVS	TET (Deng et al. 2022)	VGGsNN	-	-	9.54	77.33
	STP (Ma et al. 2025)	VGG11	-	-	113.00	78.50
	STL-SNN (Sun et al. 2023)	ConvFC	-	-	1.53	77.30
	Spikformer <sup>†</sup> (Zhou et al. 2023b)	Spikformer-2-256-1024	-	-	2.59/1.58	<b>80.90</b>
	CML (Zhou et al. 2023a)	Spikformer-2-256-1024	-	-	2.57/1.58	79.20
	L <sub>1</sub> P+sLIF (ours)	Spikformer-2-256-1024	80	48.65/79.75	1.33/0.32	78.00(-2.90)
	L <sub>1</sub> P+sLIF (ours)	Spikformer-2-256-1024	90	54.83/89.87	1.17/0.16	76.30(-4.60)
	DSP+sLIF (ours)	Spikformer-2-48-204	80	49.03/80.38	1.32/0.31	77.20(-3.70)
	DSP+sLIF (ours)	Spikformer-2-16-102	90	55.60/91.14	<b>1.15/0.14</b>	77.30(-3.60)

Table 2: Classification results on the CIFAR10 and CIFAR10-DVS datasets. Symbol <sup>†</sup> represents the baseline model.

by a substantial compression ratio of 60.62%/79.94%, and a significantly reduced parameter count of 3.67M/1.42M. When the sparsity is further increased to  $p = 90\%$ , the model maintains a competitive accuracy of 92.32%, while the parameter count is further reduced to 2.96M/0.71M. Similarly, the proposed DSP+sLIF strategy also demonstrates strong performance with enhanced parameter efficiency, achieving 93.14% (92.23%) accuracy with only 3.71M (3.02M) parameters under  $p = 80\%$  ( $p = 90\%$ ).

**Neuromorphic Datasets Classification** On the CIFAR10-DVS dataset, the proposed lightweight models also demonstrate competitive performance, as summarized in Tab. 2. The baseline Spikformer model achieves an accuracy of 80.90% with 2.59M/1.58M parameters. By applying the L<sub>1</sub>P+sLIF method under a sparsity level of  $p = 80\%$ , the model is compressed to 1.33M/0.32M parameters while maintaining a commendable accuracy of 78.00%. Similarly, the DSP+sLIF strategy yields a compact model with the Spikformer-2-48-204 architecture, with only 1.32M/0.31M parameters and an accuracy of 77.20% under

the same sparsity level. The performance is similar while increasing the sparsity level.

## Ablation Analysis

**Performance under different level of sparsity** To comprehensively evaluate the performance of the proposed lightweight strategies, we perform pruning experiments at varying pruning sparsity (denoted as “sLIF”). For comparison, we also assess the accuracy of the original model after pruning (denoted as “Pruned”). Additionally, to evaluate the contribution of synergistic learning, we conduct pruning experiments while retaining the original LIF neurons (denoted as “LIF”). As illustrated in Fig. 4, model accuracy generally declines after pruning, with greater sparsity levels resulting in more pronounced performance degradation. Compared to the unstructured pruning strategy (L<sub>1</sub>P), the structured pruning approach (DSP) causes more substantial performance deterioration, which is consistent with prior findings. Nonetheless, fine-tuning is consistently an efficient strategy to recover performance. Notably, models fine-tuned



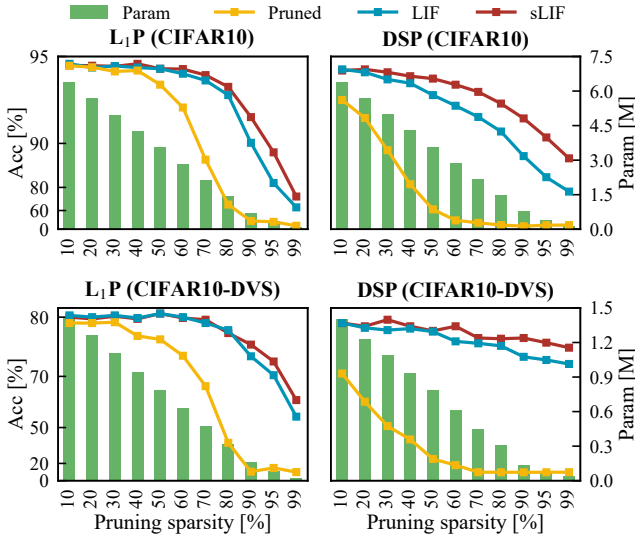


Figure 4: Performance on the CIFAR10 and CIFAR10-DVS datasets under varying levels of pruning sparsity.

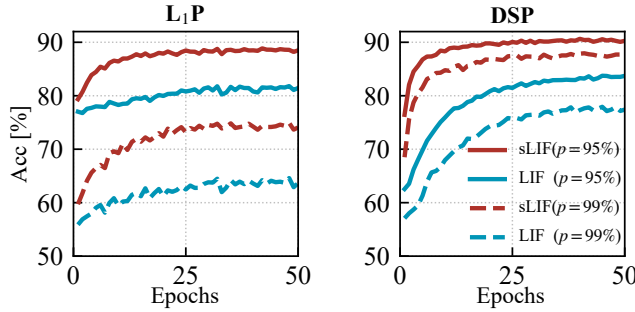


Figure 5: Convergence curves of pruned models on the CIFAR10 dataset during fine-tuning phase.

with synergistic learning exhibit superior performance recovery, with the benefits of synergistic learning becoming increasingly evident at higher sparsity levels.

In addition to superior compensation performance, the convergence speed during the fine-tuning process is a critical factor in evaluating the effectiveness of a compensation strategy. We present the accuracy curves for the ‘sLIF’ and ‘LIF’ models under pruning sparsity of  $p = 0.99\%$  and  $p = 0.95\%$  on the CIFAR10 dataset, as shown in Fig. 5. In our experiments, we configured the fine-tuning process to run for 50 epochs. Across models pruned with various strategies, the sLIF approach consistently enables faster convergence during fine-tuning. Notably, this advantage is particularly pronounced for models pruned using the DSP method. Specifically, models fine-tuned with sLIF achieve convergence in approximately 20 epochs, whereas the ablation group employing LIF neurons requires around 40 epochs to reach convergence.

**Impact on Model Inference Performance** Inference latency and energy consumption represent two fundamental metrics for assessing the inference performance of mod-

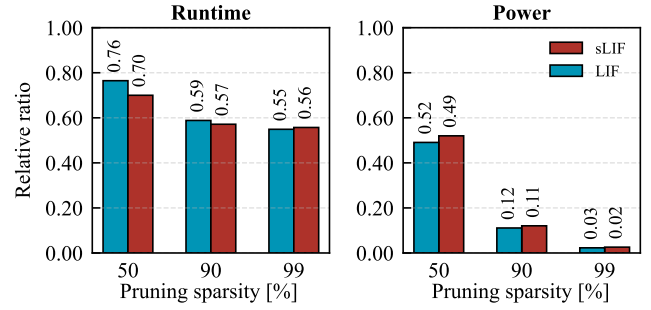


Figure 6: Relative ratio of runtime and theoretical power consumption of the lightweight models compared to the baseline models.

els. Given that structured pruning facilitates improved hardware accessibility, we evaluate the average batch inference runtime and theoretical power consumption of the DSP+LIF and DSP+sLIF models under pruning sparsity of  $p = 50\%$ ,  $90\%$ , and  $99\%$ , respectively. The relative ratios of the lightweight models compared to their corresponding baseline models are presented in Fig. 6.

As the number of parameters decreases, the inference runtime of the models consistently declines. In particular, the most compact pruned architecture, Spikformer-4-12-15, achieves an inference time that is approximately 50% of that of the baseline model. This acceleration is primarily attributed to the lower computational complexity of the lightweight models, offering promising potential for improving offline performance on edge hardware platforms.

SNN models predominantly utilize sparse accumulate operations as their primary computational units, resulting in significantly lower power consumption compared to traditional artificial neural networks. Additionally, the overall energy consumption of SNNs is influenced by both the model architecture and the neuronal firing rate. In this study, we estimate theoretical energy consumption following the method used in prior work (Yao et al. 2023b; Sun et al. 2024). As shown in Fig. 6, the relative energy consumption of pruned models, compared to the baseline, shows a positive correlation with the number of model parameters. Furthermore, sLIF models demonstrate slightly higher energy consumption than their LIF counterparts.

**Visualization of Attention Maps** In the DSP+sLIF models, the dimensions of the  $Q$ ,  $K$ , and  $V$  representations are reduced to extremely low levels. For instance, pruning the original ‘Spikformer-8-512-2048’ architecture (Tab. 1) with a pruning sparsity of  $p = 90\%$  results in a lightweight ‘Spikformer-8-48-204’ model, where only 48 dimensions are used to represent the patch embeddings. Example attention maps at the final time step are shown in Fig. 7. Despite the reduced dimensionality, the lightweight model still effectively captures image regions relevant to classification tasks. These results demonstrate that our compensation strategy is an efficient and effective approach for compressing ST-based models. Detailed visualization method and further examples are provided in the Appendix.

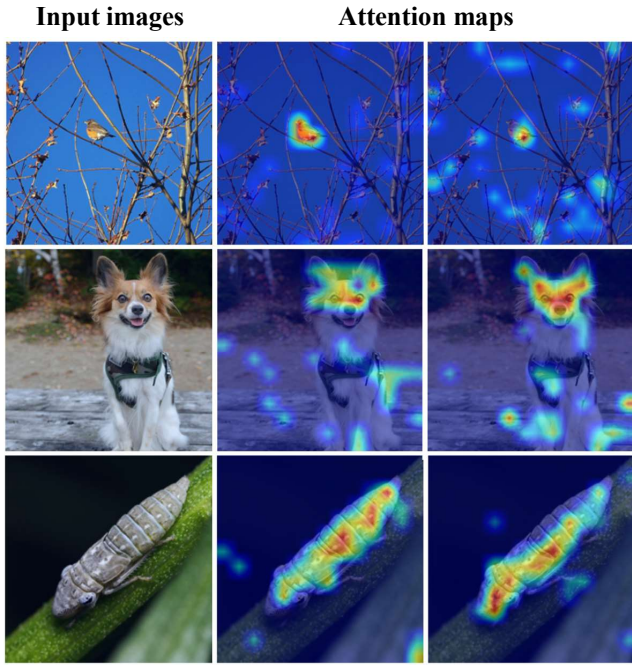


Figure 7: Representative examples of attention maps generated by the original (middle) and lightweight (right) models.

Sparsity	baseline	$p=30\%$	$p=50\%$	$p=90\%$
Param [M]	29.71	22.05	17.12	7.00
Acc [%]	72.86	67.70	65.02	56.00

Table 3: Performance on the ImageNet-1k dataset.

### The Evolutionary Process of IP Parameters

To evaluate the contribution of IP parameters to model performance, we visualize the evolution of the  $u_{th}$  and  $\tau$  associated with the  $Q$  embedding in the first ST block on the CIFAR10 and CIFAR10-DVS datasets. As illustrated in Fig. 8, the magnitude of IP parameter adaptation is positively correlated with the sparsity level. Moreover, the evolution is more pronounced on the more challenging CIFAR10-DVS dataset. These results indicate that IP parameters play a more significant role in enhancing model performance under increased task difficulty. More results on the  $K$  and  $V$  embeddings can be found in the Appendix, which demonstrate similar conclusions.

### Performance on the Large-Scale Dataset

We conduct experiments with the DSP+sLIF method on the more challenging ImageNet-1K dataset (Tab. 3). The model architecture and experimental settings are aligned with those used for ImageNet-100. Compared to ImageNet-100, a more significant performance drop is observed at high sparsity levels (e.g., 16.86% on ImageNet-1K vs. 2.48% on ImageNet-100 at  $p = 90\%$ ). This degradation is theoretically reasonable, as larger-scale datasets require larger model size according to scaling laws (Dosovitskiy et al. 2021). Nevertheless, the DSP+sLIF method remains ef-

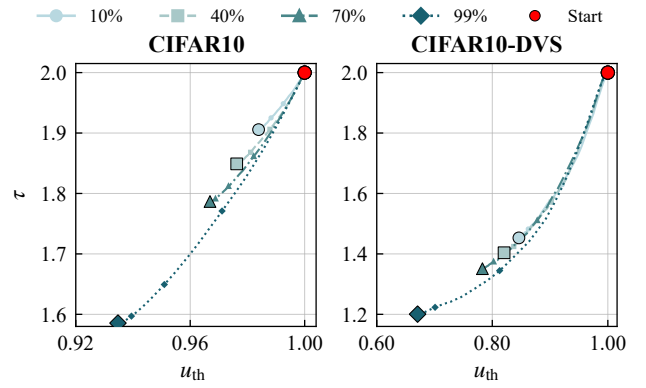


Figure 8: Evolution of IP parameters of the  $Q$  embedding. 'Start' indicates the initial parameter values.

Method	ST	Param [M]	mIoU [%]
MetaFormer (Yu et al. 2022)	×	15.50	32.90
DeeplabV3 (Zhang et al. 2022b)	×	68.10	42.10
SDTv2 <sup>†</sup> (Yao et al. 2024)	✓	9.42	30.14
DSP+sLIF (ours)	✓	4.70	26.69

Table 4: Semantic segmentation on the ADE20K dataset.

fective, achieving competitive performance under extreme compression even on large-scale datasets.

### Performance on the Downstream Tasks

To further demonstrate the effectiveness of the proposed DSP+sLIF method on complex downstream tasks, we apply it to semantic segmentation. The ST-based SDTv2 models (Yao et al. 2024) are used as the baseline, and the DSP+sLIF strategy is employed to compress the original models with a pruning sparsity of  $p = 90\%$ . As shown in Tab. 4, the resulting lightweight ST-based semantic segmentation model achieves 26.69% mIoU performance while requiring only 4.70M parameters. The qualitative visualization and discussion can be found in the Appendix.

### Conclusion

In this work, we propose combining synapse pruning and synergistic learning-based information compensation to enhance efficient ST-based models. Specifically, we introduce two synapse pruning strategies—unstructured and structured—tailored to transformer blocks in SNN models to derive compact ST-based architectures. During the fine-tuning phase, synergistic learning is applied to models incorporating sLIF neurons to compensate post-pruning performance. The model size can be flexibly controlled by specifying the desired sparsity level. Experimental results demonstrate that the proposed method effectively compresses various ST-based models. Furthermore, the resulting lightweight models exhibit improved inference performance, underscoring their potential for deployment in edge computing systems.

## Acknowledgments

This work was supported in part by the National Key Research and Development Program of China (2023YFF1204200), in part by the STI 2030–Major Projects (2022ZD0208500), and in part by the Sichuan Science and Technology Program (2024NSFTD0032, 2024NSFJQ0004, and DQ202410).

## References

- Abnar, S.; and Zuidema, W. 2020. Quantifying Attention Flow in Transformers. In *Annual Meeting of the Association for Computational Linguistics*.
- Achiam, J.; Adler, S.; Agarwal, S.; Ahmad, L.; Akkaya, I.; Aleman, F. L.; Almeida, D.; Altenschmidt, J.; Altman, S.; Anadkat, S.; et al. 2023. GPT-4 Technical Report. *arXiv preprint arXiv:2303.08774*.
- Chen, Y.; Mai, Y.; Feng, R.; and Xiao, J. 2022. An Adaptive Threshold Mechanism for Accurate and Efficient Deep Spiking Convolutional Neural Networks. *Neurocomputing*, 469: 189–197.
- Chun-Hsiao Yeh, Y. C. 2022. IN100PyTorch: PyTorch Implementation: Training ResNets on ImageNet-100. <https://github.com/danielchyeh/ImageNet-100-Pytorch>.
- Datta, G.; Liu, Z.; Li, A.; and Beerel, P. A. 2025. Dynamic SpikFormer: Low-Latency and Energy-Efficient Spiking Neural Networks with Dynamic Time Steps for Vision Transformers. In *2025 IEEE International Conference on Acoustics, Speech and Signal Processing*, 1–5.
- Davies, S.; Gait, A.; Rowley, A.; and Di Nuovo, A. 2025. Supervised Learning of Spatial Features with STDP and Homeostasis using Spiking Neural Networks on SpiNNaker. *Neurocomputing*, 611: 128650.
- Deng, J.; Dong, W.; Socher, R.; Li, L.-J.; Li, K.; and Fei-Fei, L. 2009. ImageNet: A Large-Scale Hierarchical Image Database. In *2009 IEEE Conference on Computer Vision and Pattern Recognition*, 248–255.
- Deng, S.; Li, Y.; Zhang, S.; and Gu, S. 2022. Temporal Efficient Training of Spiking Neural Network via Gradient Reweighting. In *International Conference on Learning Representations*.
- Devlin, J.; Chang, M.-W.; Lee, K.; and Toutanova, K. 2019. BERT: Pre-training of deep bidirectional transformers for language understanding. In *Proceedings of the 2019 conference of the North American chapter of the association for computational linguistics: human language technologies*, 4171–4186.
- Ding, Z.; Zhao, R.; Zhang, J.; Gao, T.; Xiong, R.; Yu, Z.; and Huang, T. 2022. Spatio-Temporal Recurrent Networks for Event-based Optical Flow Estimation. In *Proceedings of the AAAI conference on artificial intelligence*, volume 36, 525–533.
- Dosovitskiy, A.; Beyer, L.; Kolesnikov, A.; Weissenborn, D.; Zhai, X.; Unterthiner, T.; Dehghani, M.; Minderer, M.; Heigold, G.; Gelly, S.; Uszkoreit, J.; and Houslsby, N. 2021. An Image is Worth 16x16 Words: Transformers for Image Recognition at Scale. In *International Conference on Learning Representations*.
- Fang, W.; Chen, Y.; Ding, J.; Yu, Z.; Masquelier, T.; Chen, D.; Huang, L.; Zhou, H.; Li, G.; and Tian, Y. 2023. Spiking-Jelly: An open-source machine learning infrastructure platform for spike-based intelligence. *Science Advances*, 9(40): eadi1480.
- Fang, W.; Yu, Z.; Chen, Y.; Masquelier, T.; Huang, T.; and Tian, Y. 2021. Incorporating learnable membrane time constant to enhance learning of spiking neural networks. In *Proceedings of the IEEE/CVF international conference on computer vision*, 2661–2671.
- Hasssan, A.; Meng, J.; Anupreetham, A.; and Seo, J.-s. 2024. IM-SNN: Memory-Efficient Spiking Neural Network with Low-Precision Membrane Potentials and Weights. In *2024 International Conference on Neuromorphic Systems (ICONS)*, 148–155. IEEE.
- Huang, Z.; Shi, X.; Hao, Z.; Bu, T.; Ding, J.; Yu, Z.; and Huang, T. 2024. Towards High-Performance Spiking Transformers from ANN to SNN Conversion. In *Proceedings of the 32nd ACM international conference on multimedia*, 10688–10697.
- Kang, D.; Lee, Y.; Lee, E.-K.; Kang, B.; Lee, J.; and Baek, H. 2024. AT-SNN: Adaptive Tokens for Vision Transformer on Spiking Neural Network. *arXiv preprint arXiv:2408.12293*.
- Kim, S.; Kim, S.; Jo, W.; Kim, S.; Hong, S.; Lee, N.; Lee, J.; and Yoo, H.-J. 2025. C-Transformer: An Energy-Efficient Homogeneous DNN-Transformer/SNN-Transformer Processor for Large Language Models. *IEEE Journal of Solid-State Circuits*.
- Kim, Y.; Li, Y.; Moitra, A.; Yin, R.; and Panda, P. 2023. Sharing Leaky-Integrate-and-Fire Neurons for Memory-Efficient Spiking Neural Networks. *Frontiers in Neuroscience*, Volume 17 - 2023.
- Krizhevsky, A.; Hinton, G.; et al. 2009. Learning Multiple Layers of Features from Tiny Images.
- Li, H.; Liu, H.; Ji, X.; Li, G.; and Shi, L. 2017. CIFAR10-DVS: An Event-Stream Dataset for Object Classification. *Frontiers in neuroscience*, 11: 244131.
- Li, Y.; and Li, C. 2013. Synergies Between Intrinsic and Synaptic Plasticity based on Information Theoretic Learning. *PloS One*, 8(5): e62894.
- Liu, Q.; Xing, D.; Tang, H.; Ma, D.; and Pan, G. 2021. Event-based Action Recognition Using Motion Information and Spiking Neural Networks. In *Proceedings of the Thirtieth International Joint Conference on Artificial Intelligence*, 1743–1749.
- Lu, C.; Du, H.; Wei, W.; Sun, Q.; Wang, Y.; Zeng, D.; Chen, W.; Zhang, M.; and Yang, Y. 2025. ESTSformer: Efficient Spatio-Temporal Spiking Transformer. *Neural Networks*, 191: 107786.
- Ma, C.; Chen, X.; Li, Y.; Yang, Q.; Wu, Y.; Li, G.; Pan, G.; Tang, H.; Tan, K. C.; and Wu, J. 2025. Spiking Neural Networks for Temporal Processing: Status Quo and Future Prospects. *arXiv preprint arXiv:2502.09449*.



- Mukhoty, B.; Bojkovic, V.; de Vazelhes, W.; Zhao, X.; De Masi, G.; Xiong, H.; and Gu, B. 2023. Direct Training of SNN using Local Zeroth Order Method. *Advances in Neural Information Processing Systems*, 36: 18994–19014.
- Pazderka, A. 2024. *The Role of Membrane Time Constant in The Training of Spiking Neural Networks*. Ph.D. thesis, Delft University of Technology.
- Perez-Nieves, N.; Leung, V. C.; Dragotti, P. L.; and Goodman, D. F. 2021. Neural Heterogeneity Promotes Robust Learning. *Nature Communications*, 12(1): 5791.
- Qiu, X.; Zhang, J.; Wei, W.; Cao, H.; Guo, J.; Zhu, R.-J.; Shan, Y.; Yang, Y.; Zhang, M.; and Li, H. 2025. Quantized Spike-driven Transformer. In *The Thirteenth International Conference on Learning Representations*.
- Shen, H.; Zheng, Q.; Wang, H.; and Pan, G. 2024. Rethinking the Membrane Dynamics and Optimization Objectives of Spiking Neural Networks. *Advances in Neural Information Processing Systems*, 37: 92697–92720.
- Sun, H.; Cai, W.; Yang, B.; Cui, Y.; Xia, Y.; Yao, D.; and Guo, D. 2023. A Synapse-Threshold Synergistic Learning Approach for Spiking Neural Networks. *IEEE Transactions on Cognitive and Developmental Systems*, 16(2): 544–558.
- Sun, H.; Liu, R.; Cai, W.; Wang, J.; Wang, Y.; Tang, H.; Cui, Y.; Yao, D.; and Guo, D. 2024. Reliable Object Tracking by Multimodal Hybrid Feature Extraction and Transformer-based Fusion. *Neural Networks*, 178: 106493.
- Touvron, H.; Lavril, T.; Izacard, G.; Martinet, X.; Lachaux, M.-A.; Lacroix, T.; Rozière, B.; Goyal, N.; Hambro, E.; Azhar, F.; et al. 2023. LLaMA: Open and Efficient Foundation Language Models. *arXiv preprint arXiv:2302.13971*.
- Vaswani, A.; Shazeer, N.; Parmar, N.; Uszkoreit, J.; Jones, L.; Gomez, A. N.; Kaiser, Ł.; and Polosukhin, I. 2017. Attention is All You Need. *Advances in neural information processing systems*, 30.
- Wang, Q.; Zhang, T.; Han, M.; Wang, Y.; Zhang, D.; and Xu, B. 2023. Complex Dynamic Neurons Improved Spiking Transformer Network for Efficient Automatic Speech Recognition. In *Proceedings of the AAAI conference on artificial intelligence*, volume 37, 102–109.
- Wang, S.; Zhang, M.; Zhang, D.; Belatreche, A.; Xiao, Y.; Liang, Y.; Shan, Y.; Sun, Q.; Zhang, E.; and Yang, Y. 2025. Spiking Vision Transformer with Saccadic Attention. In *The Thirteenth International Conference on Learning Representations*.
- Wu, Y.; Deng, L.; Li, G.; Zhu, J.; and Shi, L. 2018. Spatio-Temporal Backpropagation for Training High-Performance Spiking Neural Networks. *Frontiers in neuroscience*, 12: 331.
- Yao, M.; Hu, J.; Hu, T.; Xu, Y.; Zhou, Z.; Tian, Y.; XU, B.; and Li, G. 2024. Spike-driven Transformer V2: Meta Spiking Neural Network Architecture Inspiring the Design of Next-generation Neuromorphic Chips. In *The Twelfth International Conference on Learning Representations*.
- Yao, M.; Hu, J.; Zhou, Z.; Yuan, L.; Tian, Y.; Xu, B.; and Li, G. 2023a. Spike-driven Transformer. *Advances in neural information processing systems*, 36: 64043–64058.
- Yao, M.; Zhang, H.; Zhao, G.; Zhang, X.; Wang, D.; Cao, G.; and Li, G. 2023b. Sparser Spiking Activity Can Be Better: Feature Refine-and-Mask Spiking Neural Network for Event-based Visual Recognition. *Neural Networks*, 166: 410–423.
- Yu, W.; Luo, M.; Zhou, P.; Si, C.; Zhou, Y.; Wang, X.; Feng, J.; and Yan, S. 2022. Metaformer is Actually What You Need for Vision. In *Proceedings of the IEEE/CVF conference on computer vision and pattern recognition*, 10819–10829.
- Zhang, A.; Li, X.; Gao, Y.; and Niu, Y. 2022a. Event-Driven Intrinsic Plasticity for Spiking Convolutional Neural Networks. *IEEE Transactions on Neural Networks and Learning Systems*, 33(5): 1986–1995.
- Zhang, H.; Wu, C.; Zhang, Z.; Zhu, Y.; Lin, H.; Zhang, Z.; Sun, Y.; He, T.; Mueller, J.; Manmatha, R.; et al. 2022b. Resnest: Split-Attention Networks. In *Proceedings of the IEEE/CVF conference on computer vision and pattern recognition*, 2736–2746.
- Zhang, J.; Zhang, M.; Wang, Y.; Liu, Q.; Yin, B.; Li, H.; and Yang, X. 2025. Spiking Neural Networks With Adaptive Membrane Time Constant for Event-Based Tracking. *IEEE Transactions on Image Processing*, 34: 1009–1021.
- Zheng, H.; Wu, Y.; Deng, L.; Hu, Y.; and Li, G. 2021. Going Deeper with Directly-Trained Larger Spiking Neural Networks. In *Proceedings of the AAAI conference on artificial intelligence*, volume 35, 11062–11070.
- Zheng, H.; Zheng, Z.; Hu, R.; Xiao, B.; Wu, Y.; Yu, F.; Liu, X.; Li, G.; and Deng, L. 2024. Temporal Dendritic Heterogeneity Incorporated with Spiking Neural Networks for Learning Multi-Timescale Dynamics. *Nature Communications*, 15(1): 277.
- Zhou, B.; Zhao, H.; Puig, X.; Fidler, S.; Barriuso, A.; and Torralba, A. 2017. Scene Parsing Through ADE20K Dataset. In *Proceedings of the IEEE conference on computer vision and pattern recognition*, 633–641.
- Zhou, C.; Zhang, H.; Zhou, Z.; Yu, L.; Huang, L.; Fan, X.; Yuan, L.; Ma, Z.; Zhou, H.; and Tian, Y. 2024a. QKFormer: Hierarchical Spiking Transformer using Q-K Attention. In *The Thirty-eighth Annual Conference on Neural Information Processing Systems*.
- Zhou, C.; Zhang, H.; Zhou, Z.; Yu, L.; Ma, Z.; Zhou, H.; Fan, X.; and Tian, Y. 2023a. Enhancing the Performance of Transformer-based Spiking Neural Networks by Improved Downsampling with Precise Gradient Backpropagation. *arXiv:2305.05954*.
- Zhou, Z.; Che, K.; Niu, J.; Yao, M.; Li, G.; Yuan, L.; Luo, G.; and Zhu, Y. 2024b. Spatial-Temporal Spiking Feature Pruning in Spiking Transformer. *IEEE Transactions on Cognitive and Developmental Systems*.
- Zhou, Z.; Zhu, Y.; He, C.; Wang, Y.; YAN, S.; Tian, Y.; and Yuan, L. 2023b. Spikformer: When Spiking Neural Network Meets Transformer. In *The Eleventh International Conference on Learning Representations*.

## Appendix

### Related Work

#### Efficient Spiking Transformer

ST-based models have garnered significant attention due to their potential for biologically plausible computation and energy-efficient processing of spatio-temporal data (Zhou et al. 2023b; Yao et al. 2023a). However, the high computational cost and memory overhead inherent in their complex dynamics necessitate efficiency-oriented enhancements. Prior work can be broadly categorized into structure-oriented and engineering-oriented approaches. **Structure-Oriented Optimization:** A primary direction for improving efficiency in ST blocks lies in architectural redesign. Inspired by model pruning strategies, researchers have explored eliminating redundant spatial and temporal components in attention mechanisms and feedforward layers, thereby reducing computational burden without substantially degrading accuracy (Zhou et al. 2024b; Kang et al. 2024). Another line of work proposes meta-architecture redesigns (Yao et al. 2024; Wang et al. 2025), which tailor model structures to the unique characteristics of spiking data. Furthermore, the integration of lightweight functional modules—such as linearized QK-value embedding and simplified gating mechanisms—has shown promise in improving representational efficiency with minimal performance trade-offs (Zhou et al. 2024a; Datta et al. 2025; Lu et al. 2025). **Engineering-Oriented Solutions:** In parallel, engineering-based methods addressing practical deployment issues have been proposed. Weight quantization, which reduces numerical precision, is a widely used technique to enable model deployment on edge devices. Researchers have incorporated quantization-aware training into ST-based models to lower the bit-width of weights and activations, thereby minimizing memory footprint and enabling deployment on low-power hardware (Qiu et al. 2025). Similarly, advances in specialized neuromorphic hardware—such as event-driven computing cores and custom-designed crossbar arrays—have significantly reduced latency and energy consumption for ST-based models (Kim et al. 2025). Despite their success, these methods tend to be model-dependent or require non-trivial system-level integration. This lack of universality limits their adaptability to diverse architectures and downstream tasks.

#### Bio-Inspired Spiking Neuron Models

The spiking neuron, as the fundamental computational unit, plays a critical role in determining the overall performance of SNNs (Zheng et al. 2024). Among various neuron models, the LIF model is one of the most widely adopted due to its simplicity and computational efficiency. By training LIF neurons with **synaptic plasticity** mechanisms (Wu et al. 2018; Davies et al. 2025), SNN models have achieved competitive performance on various tasks (Sun et al. 2024; Ding et al. 2022; Liu et al. 2021). Despite these advantages, the limited representational capacity of LIF in capturing complex spatio-temporal dynamics has motivated the development of more biologically inspired neuron models. In spiking neurons, **intrinsic parameters** (i.e., the membrane time constant, firing threshold, and resting potential) play a crucial role in shaping internal dynamics, including input integration, spike generation, and the refractory period (Zhang et al. 2022a). Based on the biological mechanisms underlying the firing threshold, numerous enhanced variants of the LIF model have been proposed, focusing on the threshold adaptation, dynamic thresholds, and subthreshold dynamics (Sun et al. 2023; Huang et al. 2024; Chen et al. 2022). Compared to the standard LIF neuron, these models offer a more biologically plausible depiction of threshold behavior, thereby enhancing the neuron’s ability to robustly represent spatial patterns. Furthermore, the membrane time constant governs the temporal integration of incoming signals (Pazderka 2024). By introducing heterogeneity in this parameter, recent studies have significantly improved the capacity of SNNs to capture spatial features across multiple time scales (Fang et al. 2021; Perez-Nieves et al. 2021; Zhang et al. 2025). A key challenge in enhancing LIF neuron models lies in the effective integration of the **synergistic interactions** between synaptic and intrinsic parameters. Prior studies have typically treated these parameters as independent components or optimized them using information-theoretic approaches, often overlooking their interdependence (Li and Li 2013). This not only limits the model expressiveness but also complicates the training process. Therefore, two critical questions remain open: how to incorporate synaptic and intrinsic plasticity in a unified and efficient framework, and how to enable synergistic learning between these two forms of plasticity.

### Experimental Details

This appendix provides detailed information about the experimental setup used to evaluate our method, including datasets, implementation frameworks, hardware specifications, and configuration details.

#### Datasets

To comprehensively evaluate the performance and generalization capability of the proposed method across both static and neuromorphic vision tasks, we utilize a diverse set of benchmark datasets. Below, we provide detailed descriptions of each dataset, highlighting their composition, key characteristics, and relevance to our experimental settings.

- **ImageNet** (Deng et al. 2009) is a large-scale static image dataset widely used for object recognition tasks, comprising approximately 1.28 million training images and 50,000 validation images across 1,000 classes. In our experiments, all images are resized to a resolution of  $224 \times 224$  pixels for consistency. To evaluate the classification performance of our method on high-resolution static images, we adopt the ImageNet-100 subset (Chun-Hsiao Yeh 2022), where the classes are

Hyper-parameter	ImageNet	CIFAR10	CIFAR10-DVS	ADE20K
Epochs/iterations	50	50	56	200000
Warmup epochs	20	0	10	1500
Batch size	64	128	16	16
Optimizer	AdamW	AdamW	AdamW	AdamW
Initial Learning rate	0.0001	0.00001	0.0001	0.001
Learning rate decay	Cosine	Cosine	Cosine	LinearLR
Weight decay	0.05	0.06	0.06	0.005
Time steps	4	4	16	4
Resolution	224×224	32×32	128×128	512×512
Patch size	16	4	16	16

Table S5: Configuration Parameters for Experiments

selected following prior work. This subset serves as a benchmark for comparison with state-of-the-art (SOTA) models in conventional computer vision tasks. Additionally, the full ImageNet-1K dataset is employed to assess the scalability of our method under the scaling-law setting.

- **CIFAR-10** (Krizhevsky, Hinton et al. 2009) is a static image dataset consisting of 50,000 training images and 10,000 test images, each with a resolution of  $32 \times 32$  pixels and evenly distributed across 10 classes. It is used to evaluate the effectiveness of our method on low-resolution static images, offering a lightweight yet challenging benchmark for classification tasks.
- **CIFAR10-DVS** (Li et al. 2017) is a neuromorphic dataset derived from the original CIFAR-10, recorded using a dynamic vision sensor (DVS). It comprises event streams from 10,000 samples spanning the same 10 classes as CIFAR-10, where each sample is represented as a sequence of address-event representations (AER) instead of conventional image frames. With temporal resolution on the order of microseconds, this dataset is well-suited for evaluating the performance of our method on event-based, neuromorphic vision tasks. In our experiments, each event stream is temporally averaged and segmented into 16 discrete time steps.
- **ADE20K** (Zhou et al. 2017) is a widely used dataset for semantic segmentation, comprising 20,210 training images and 2,000 validation images annotated with 150 semantic categories. For segmentation tasks, images are typically resized to a resolution of  $512 \times 512$  pixels. Owing to its diverse scene compositions and fine-grained annotations, ADE20K serves as a benchmark to assess the generalization capability of our method on downstream tasks, particularly semantic segmentation.

## Computing Infrastructure

All experiments are conducted on a machine with the following hardware and software configurations:

- **Hardware:**
  - **GPU:**  $4 \times$  NVIDIA A800 80GB
  - **CPU:** Intel(R) Xeon(R) Gold 6348 CPU @ 2.60GHz
  - **Memory:** 160 GB RAM
- **Software:**
  - **Operating System:** CentOS Linux 7 (Core)
  - **Python Version:** Python 3.8.20
  - **Deep Learning Frameworks:** PyTorch 1.10.0+cu111 and SpikingJelly 0.0.0.12

The same environment is used for all experiments to ensure reproducibility.

## Configuration Details

Tab. S5 summarizes the key configuration parameters used for each dataset in our experiments.

## Additional Results and Analysis

### Effectiveness of Pruning Methods

To enable efficient model pruning, accurately evaluating the importance of individual components within the model is essential. In the proposed  $\mathbf{L}_1\mathbf{P}$  method, which is designed for constructing sparse weight matrices, the  $\mathbf{L}_1$  norm is employed to quantify the significance of each matrix element. Elements are then pruned based on their ranking derived from the  $\mathbf{L}_1$  importance scores. As illustrated in Fig. S9, under a pruning sparsity of  $p = 90\%$ , only a small subset of elements with the highest  $\mathbf{L}_1$  importance are retained in the sparse weight matrix. To validate the effectiveness of this selection criterion, we conducted a

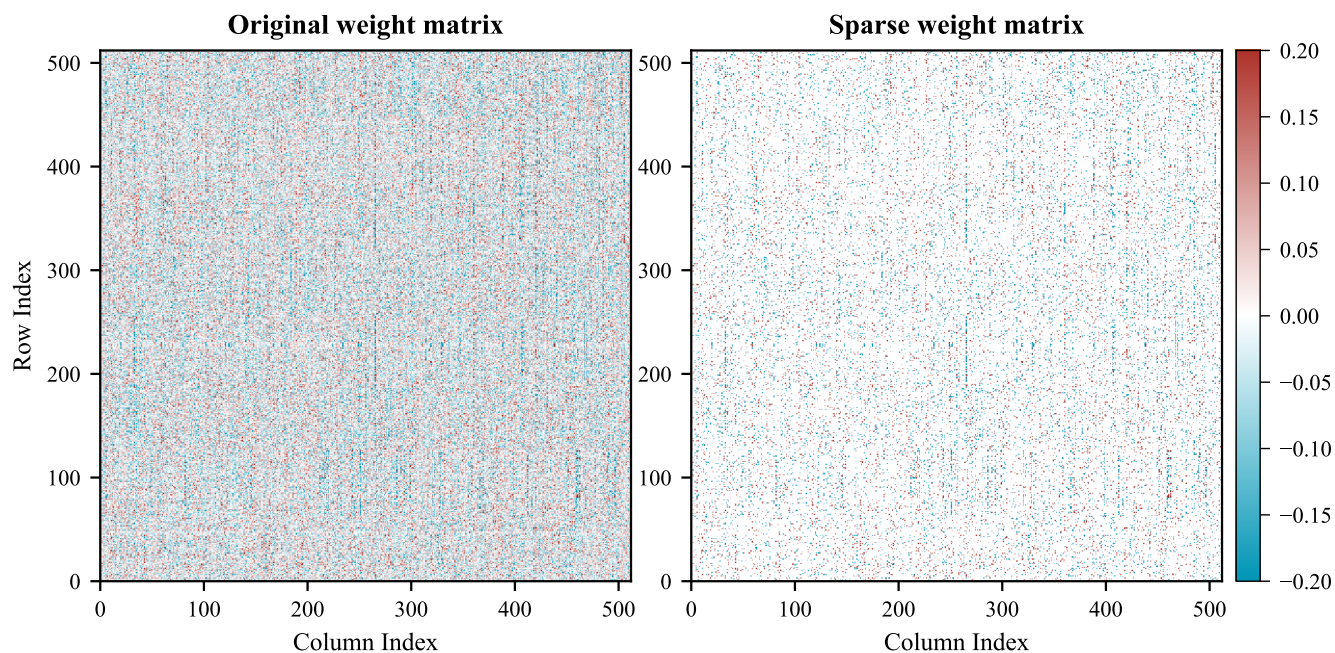


Figure S9: Visualization of the original and sparse weight matrices. Each pixel represents a value of weight elements and heavy color is correlated with a more higher absolute value.

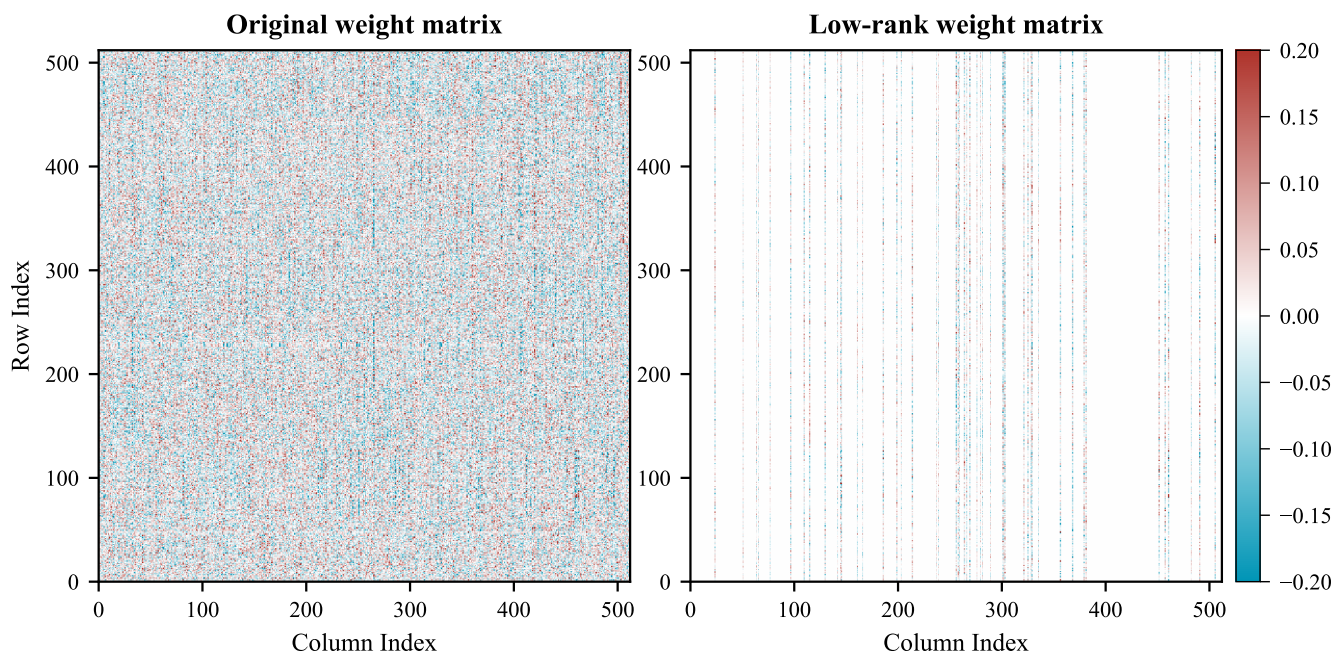


Figure S10: Visualization of the original and low-rank weight matrices. Each pixel represents a value of weight elements and heavy color is correlated with a more higher absolute value.

Pruning sparsity	Sparse weight matrix		Low-rank weight matrix	
	Random [%]	L <sub>1</sub> P [%]	Random [%]	DSP [%]
$p = 10\%$	93.97	94.72	82.50	93.33
$p = 20\%$	90.74	94.67	77.63	92.26
$p = 30\%$	84.36	94.53	69.16	89.16
$p = 40\%$	71.22	94.56	62.26	81.33
$p = 50\%$	52.68	94.03	47.00	61.76
$p = 60\%$	35.50	92.92	39.77	36.81
$p = 70\%$	31.29	87.72	38.81	28.23
$p = 80\%$	29.03	67.93	23.15	19.02
$p = 90\%$	18.77	34.89	17.42	14.17
$p = 95\%$	13.00	31.74	22.52	18.61
$p = 99\%$	10.49	16.01	17.83	18.88

Table S6: Comparison of models pruned with proposed methods and random pruning.

---

Algorithm S1: Attention Rollout Visualization

---

**Require:** Attention maps  $\{\mathbf{A}_l\}_{l=1}^L$ , where  $\mathbf{A}_l \in \mathbb{R}^{H \times P \times P}$ ,  $H$  is the number of heads,  $P$  is the number of patches

**Ensure:** Visualization mask  $\mathbf{M} \in \mathbb{R}^P$

- 1: Initialize  $\mathbf{R} = \mathbf{I}_P$  (identity matrix of size  $P$ )
  - 2: **for**  $l = 1$  to  $L$  **do**
  - 3:   Compute fused attention:  $\mathbf{A}_l^{\text{fused}} = \text{mean}(\mathbf{A}_l, \text{axis}=0) \in \mathbb{R}^{P \times P}$
  - 4:   Add residual:  $\mathbf{A}_l' = \mathbf{A}_l^{\text{fused}} + \mathbf{I}_P$
  - 5:   Normalize rows:  $\mathbf{A}_l' = \mathbf{A}_l' \oslash (\mathbf{A}_l'.\text{sum}(\text{axis}=1, \text{keepdims} = \text{True}))$
  - 6:   Update rollout:  $\mathbf{R} = \mathbf{A}_l' \cdot \mathbf{R}$
  - 7: **end for**
  - 8: Compute mask:  $\mathbf{M} = \text{mean}(\mathbf{R}, \text{axis}=0) \in \mathbb{R}^P$
  - 9: Apply threshold: Set the smallest `discard_ratio` proportion of values in  $\mathbf{M}$  to zero
  - 10: Reshape and upsample  $\mathbf{M}$  to the original image size for visualization
- 

comparative experiment in which elements are pruned randomly (Tab. S6). The results show that models pruned using the random strategy exhibit significantly lower classification accuracy compared to those pruned using the  $\mathbf{L}_1\mathbf{P}$  method. Notably, in the random pruning scenario, a sharp performance drop is observed at a pruning sparsity of  $p = 30\%$ , whereas the same level of degradation occurs at  $p = 70\%$  with the  $\mathbf{L}_1\mathbf{P}$  approach.

Similarly, in the **DSP** method, pruning is performed by eliminating dimensions with low significance scores computed using the DVA metric, resulting in a low-rank approximation of the original weight matrix (see Fig. S10). To evaluate the effectiveness of this strategy, we also performed a comparative analysis by randomly pruning dimensions. The model performance with random pruning degrades rapidly, with a noticeable accuracy drop occurring before  $p = 10\%$ , substantially earlier than the degradation point at  $p = 30\%$  observed with the **DSP** method. Moreover, across pruning sparsities of  $p \leq 60\%$ , models pruned with the **DSP** strategy consistently outperform those with random pruning. Although the post-pruned accuracy in random pruning is slightly higher than that in **DSP**, this phenomenon is reasonable given the extremely low accuracy.

In summary, the experimental results validate the effectiveness of the proposed  $\mathbf{L}_1\mathbf{P}$  and **DSP** methods, which offer principled importance metrics for unstructured and structured pruning strategies, respectively.

### Detailed Visualization Method and Further Examples

To gain insights into the decision-making process of our ST-based model, we utilize an adapted version of the Attention Rollout method (Abnar and Zuidema 2020). This technique enables us to aggregate attention across all layers and visualize the regions of the input image that significantly influence the model’s predictions. Specifically, for each layer, we compute the fused attention matrix by averaging across the attention heads (Notably, all attention matrices are selected at the final time step). We then incorporate residual connections by adding the identity matrix and normalize each row to ensure it sums to one. The rollout matrix is obtained by recursively multiplying these processed attention matrices from the first to the last layer. Given that our model employs global average pooling for classification instead of a dedicated class token, we derive the importance of each patch by averaging the rollout matrix across all tokens. To emphasize the most salient regions, we apply a thresholding mechanism that sets the smallest attention values to zero based on a predefined discard ratio (set as 0.85 in our work). Finally, the resulting mask is upsampled to the original image dimensions and overlaid on the input image to produce an intuitive visualization. The entire pipeline is shown in Algorithm. S1. We also provide more examples in Fig. S11.



### **Supplementary: The Evolutionary Process of IP Parameters**

The evolution of IP parameters for the  $Q$ ,  $K$ , and  $V$  embeddings is illustrated in Fig. S12. Overall, the magnitude of IP parameter adaptation exhibits a positive correlation with pruning sparsity across all embeddings. Notably, this evolution is more pronounced on the CIFAR10-DVS dataset. These observations indicate that the influence of intrinsic plasticity is consistently reflected across the ST blocks.

### **Qualitative Results on the ADE20K Dataset**

As illustrated in Fig. S13, the semantic segmentation performance of the lightweight model exhibits a slight degradation compared to the original model. Nonetheless, considering that the lightweight model utilizes only half the number of parameters, its performance remains competitive and acceptable for practical applications.

### **Limitations**

Our compression strategy offers flexibility in obtaining lightweight models by allowing manual configuration of the predefined pruning sparsity. However, the same pruning sparsity is applied uniformly across all ST blocks, potentially overlooking the varying contributions of different blocks to the overall model performance. As part of future work, a comprehensive evaluation metric should be developed to enable dynamic adjustment of pruning levels across ST blocks based on their relative importance. Hybrid models that integrate diverse architectural components, such as convolutional blocks, MLP blocks, and transformer blocks, have demonstrated increasing potential in addressing complex tasks. Accordingly, extending our method to support a broader range of architectures may further enhance its applicability and impact across various model designs and domains.



Figure S11: Further examples of attention maps as in Figure 6.

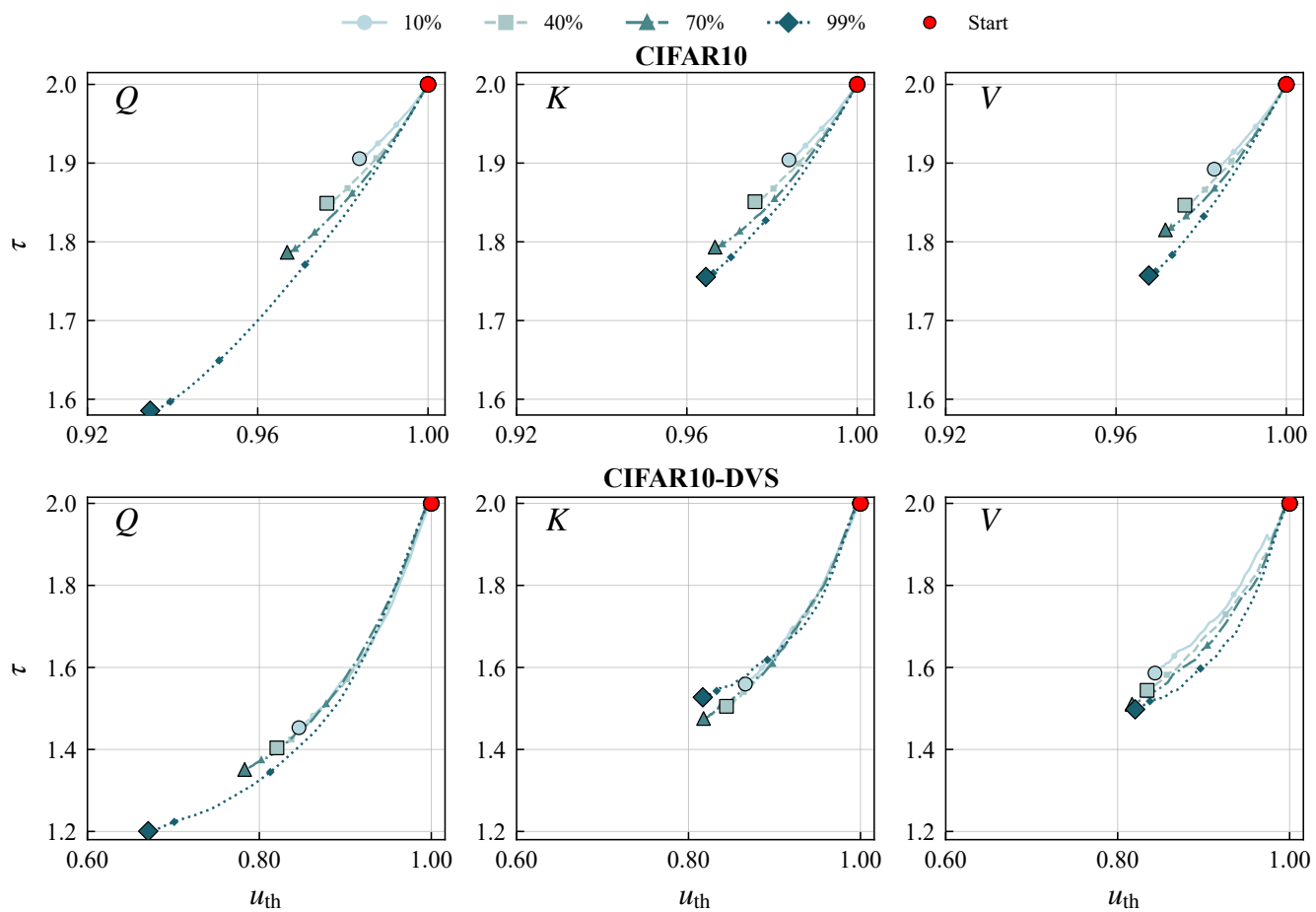


Figure S12: Evolution of IP parameters of the Q, K and V embeddings, respectively. "Start" indicates the initial parameter values.



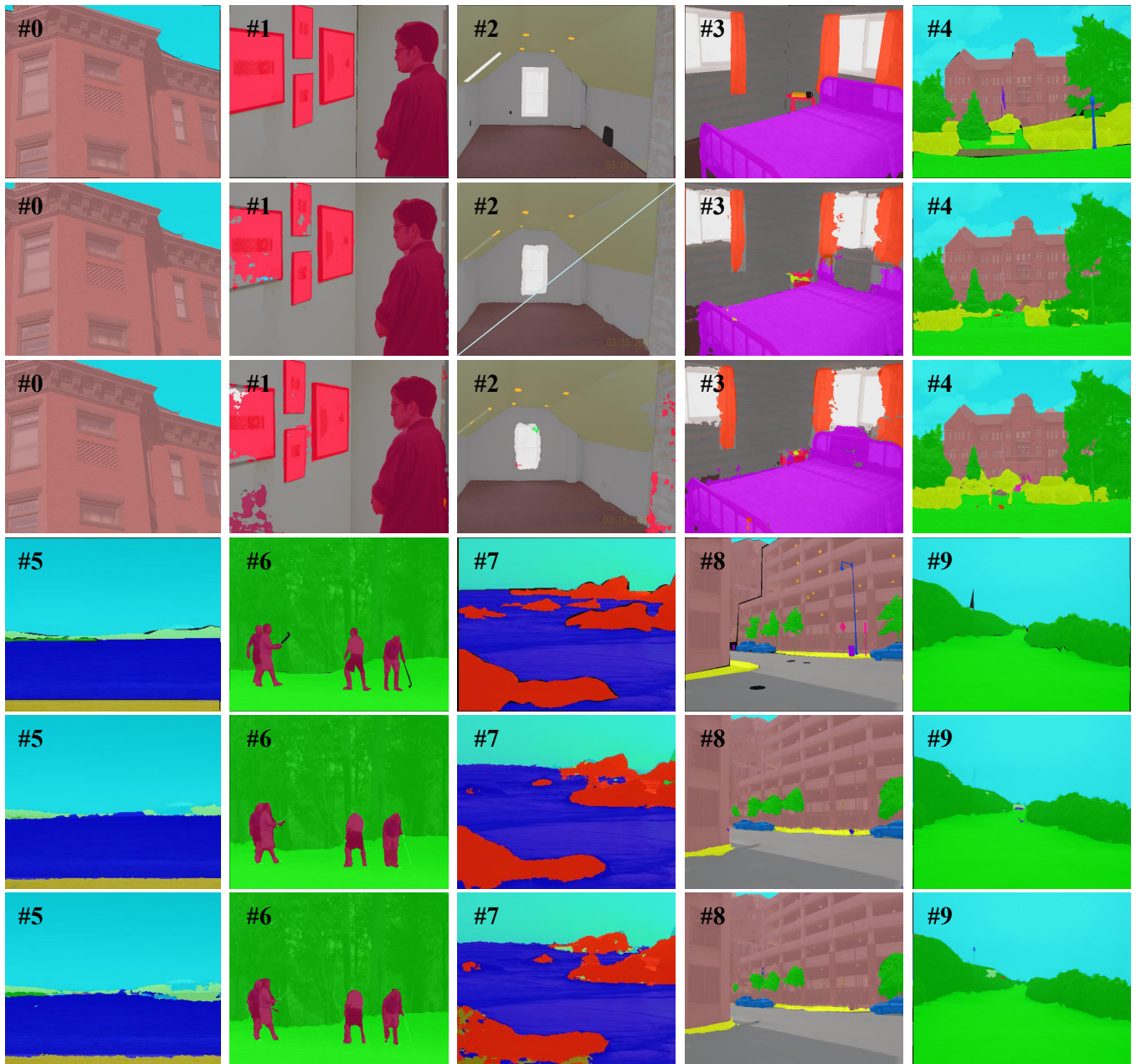


Figure S13: Qualitative semantic segmentation results on the ADE20K dataset. The top row depicts ground truth masks, while the middle and bottom rows show the predicted masks produced by the original and lightweight models, respectively.